Potassium and sodium microdomains in thin astroglial processes: A computational model study

PLOS COMPUTATIONAL BIOLOGY

RESEARCH ARTICLE

Potassium and sodium microdomains in thin astroglial processes: A computational model study

Kevin Breslin[1], John Joseph Wade[1]*, KongFatt Wong-Lin[2], Jim Harkin[1], Bronac Flanagan[1], Harm Van Zalinge[3], Steve Hall[3], Matthew Walker[4], Alexei Verkhratsky[5,6], Liam McDaid[1]

1 Computational Neuroscience and Neural Engineering (CNET) Research Team, Intelligent Systems Research Centre, Ulster University, Derry, United Kingdom, **2** Neural Systems and Neurotechnology Research Team, Intelligent Systems Research Centre, Ulster University, Derry, United Kingdom, **3** Department of Electrical Engineering and Electronics, University of Liverpool, Liverpool, United Kingdom, **4** Clinical & Experimental Epilepsy Institute of Neurology, University College London, London, United Kingdom, **5** Faculty of Biology, Medicine and Health, University of Manchester, Manchester, United Kingdom, **6** Achucarro Center for Neuroscience, IKERBASQUE, Basque Foundation for Science, Bilbao, Spain

* jj.wade@ulster.ac.uk

Citation: Breslin K, Wade JJ, Wong-Lin K, Harkin J, Flanagan B, Van Zalinge H, et al. (2018) Potassium and sodium microdomains in thin astroglial processes: A computational model study. PLoS Comput Biol 14(5): e1006151. https://doi.org/10.1371/journal.pcbi.1006151

Editor: Renaud Blaise Jolivet, University of Geneva, SWITZERLAND

Received: September 26, 2017

Accepted: April 20, 2018

Published: May 18, 2018

Data Availability Statement: All relevant data are within the paper and its Supporting Information files.

Funding: The authors received no specific funding for this work.

Competing interests: The authors have declared that no competing interests exist.

Abstract

A biophysical model that captures molecular homeostatic control of ions at the perisynaptic cradle (PsC) is of fundamental importance for understanding the interplay between astroglial and neuronal compartments. In this paper, we develop a multi-compartmental mathematical model which proposes a novel mechanism whereby the flow of cations in thin processes is restricted due to negatively charged membrane lipids which result in the formation of deep potential wells near the dipole heads. These wells restrict the flow of cations to "hopping" between adjacent wells as they transverse the process, and this surface retention of cations will be shown to give rise to the formation of potassium (K^+) and sodium (Na^+) microdomains at the PsC. We further propose that a K^+ microdomain formed at the PsC, provides the driving force for the return of K^+ to the extracellular space for uptake by the neurone, thereby preventing K^+ undershoot. A slow decay of Na^+ was also observed in our simulation after a period of glutamate stimulation which is in strong agreement with experimental observations. The pathological implications of microdomain formation during neuronal excitation are also discussed.

Author summary

During periods of neuronal activity, ionic homeostasis in the surrounding extracellular space (ECS) is disturbed. To provide a healthy environment for continued neuronal function, excess ions such as potassium must be buffered away from the ECS; a vital supportive role provided by astrocyte cells. It has long been thought that astrocytes not only removed ions from the ECS but also transport them to other areas of the brain where their concentrations are lower. However, while our computational model simulations agree that

astrocytes do remove these ions from the ECS they also show that these ions are mainly stored locally at the PsC to be returned to the ECS, thus restoring ionic homeostasis. Furthermore, we detail in this paper that this happens because of a previously overlooked biophysical phenomenon that is only dominant in thin astrocyte processes. The flow of these cations within thin processes is primarily by surface conduction where they experience the attraction of fixed negative charge at the membrane inner surface. This negative charge constrains cation movement along the surface and so their flow rate is restricted. Consequently, ions such as potassium that are released during neuronal excitation enter the PsC and are stored locally due to the low conductance pathway between the PsC and the astrocyte soma. Our simulations also show that this local build-up of K^+ is returned to the ECS after the neuronal activity dies off which could potentially explain why K^+ undershoot has not been observed; this result agrees with experimental observations. Moreover, the same mechanism can also explain the transient behaviour of Na^+ ions whereby in thin processes a slow decay time constant is experimentally observed. These findings have important implications for the role of astrocytes in regulating neuronal excitability under physiological and pathological conditions, and therefore highlight the significance of the work presented in this paper.

Introduction

Astroglia determine the architecture of neural tissue and maintain central nervous system (CNS) homeostasis [1–3]. Astrocytes are organised into functional syncytia that show anatomical specialisation [4, 5], which allow intercellular diffusion of ions, second messengers and metabolites. Astroglial membranes closely enwrap the majority of excitatory synapses in the CNS, forming astroglial cradles [6, 7]; a structure which facilitates synaptogenesis, synaptic maturation, synaptic transmission and synaptic extinction. Astroglial membranes are densely packed with transporters and ion pumps that maintain molecular homeostasis in the synaptic cleft and in the brain interstitium [8–11]. Furthermore, astrocytes maintain the homeostasis of many neurotransmitters and neuromodulators and supply neurones with glutamine, an essential precursor for the synthesis of glutamate and gamma-Aminobutric acid (GABA), the main excitatory and inhibitory neurotransmitters respectively [12–15].

K^+ homeostasis is a canonical function of astroglia proposed in the mid-1960s; both energy dependent Na^+/K^+ATPase (NKA) and passive (inward rectifier K^+ channels) pathways were considered as molecular mechanisms [9,16,17]. Subsequently the $Na^+/K^+/Cl^-$ transporter NKCC1 was suggested to participate in K^+ buffering, especially at high (pathological) K^+ concentrations [10, 18, 19]. The local K^+ uptake is supposedly supported by spatial K^+ buffering (K^+ diffusion through gap junctions from regions of elevated $[K^+]$ to regions of lower $[K^+]$).

Under physiological conditions, however, the main pathway for K^+ influx is associated with NKA, whereas $K_{ir}4.1$ inward rectifying channels mediate K^+ efflux which is needed to restore K^+ gradients in neuronal compartments [10, 18, 19]. These observations are consistent with astrocytic K^+ being re-released via $K_{ir}4.1$ channels at distal synapses after distribution in the astrocytic functional syncytium via gap junctions [18]. However, in our paper we are dealing with K^+ microdomains at the PsC, due to a low conductance pathway between the PsC and astrocyte soma, causing a significant increase in $[K^+]_{PsC}$ which returns to baseline level via K^+ leak and $K_{ir}4.1$ channels post neural excitation. Astroglial homeostatic function is, to a large extent, controlled by transmembrane Na^+ gradients and is regulated by cytoplasmic Na^+ signals [20, 21]. Dynamic fluctuations of $[Na^+]_i$ affect Na^+-dependent transporters and associated

molecular cascades that link Na^+ dynamics to homeostasis of K^+ and neurotransmitters [20, 21]. Astroglial Na^+ signals are spatially heterogeneous with the existence of Na^+ microdomains; these Na^+ signals may also propagate through astroglial syncytia via gap junctions [22]. The main pathway for astroglial Na^+ entry occurs through the excitatory amino acid transporters 1 and 2 (EAAT 1/2) [15]. Glutamate transport is powered by transmembrane ion gradients where 3 Na^+ and 1 H^+ ions are exchanged for one K^+ ion, hence the Na^+/glutamate transporter generates a net inward Na^+ current [23, 24]. In addition, glutamate opens astroglial ionotropic receptors (AMPA and NMDA receptors) and activates (indirectly through store-operated Ca^+ influx pathway) TRPC channels which further contribute to stimulus-dependent Na^+ entry [25–28]. Glutamate transporters co-localise with sodium-calcium exchanger (NCX) that couple Na^+ and Ca^{2+} signalling [29, 30].

The existence of astroglial ionic microdomains [21, 31, 32] at the PsC indicates that there must be mechanisms that slow ionic diffusion along the processes. A candidate for this mechanism is associated with fixed negative charges existing in cell membranes. Previous experiments [33] had found localised fixed negative charges in the membranes of neurones and glia. Biological membranes consist of a continuous bilayer of lipid molecules in which membrane proteins are embedded. These bilayers are filled with polar and non-polar portions in their structure (amphipathic) [34]. All eukaryotic membranes are also asymmetric such that biophysical properties differ between the intracellular and extracellular surfaces; this asymmetry is necessary for many key cellular processes including cell fusion and cell clearance [35].

As astrocyte processes are very thin we hypothesise that this effect will have a dominant role in restricting cation conduction along the membrane. Specifically, we propose that cation retention in the potential wells requires that cations must hop from well to well as they move along the thin astrocyte process and therefore, this hopping effect serves to semi-isolate the astrocytic perisynaptic cradle (PsC) from the astrocytic main body. In this paper we show, for the first time, that this slow leakage of cations could explain the formation of K^+ and Na^+ microdomains at the PsC which points to a new theory for K^+ clearance. For example, it is widely reported [9, 36] that excitatory presynaptic neurones release K^+ into the extracellular space (ECS) which is subsequently cleared at the PsC and buffered away through diffusion to the main astrocyte body. However, we propose that the flow of K^+ away from the PsC is not volume diffusion limited, but rather is restricted due to the hopping effect along the process, and therefore a K^+ microdomain forms at the PsC during sustained presynaptic neuronal excitation. Furthermore, we will show through mathematical modelling, that the formation of a K^+ microdomain at the PsC may very well be advantageous as it facilitates a low energy return pathway for K^+ to the ECS, after neuronal excitation has ceased. Additionally, cation retention along thin processes may also affect homeostasis for Na^+ ions as they also carry a positive charge. It has been shown in other work [23] that the decay rate of Na^+ following a sustained level of glutamate uptake (in the absence of extra-cellular K^+ change) through EAAT1/2 is in the order of seconds. We will also show in this paper that this could potentially result from the restricted flow rate of Na^+ ions along thin processes which results in the formation of a Na^+ microdomain at the PsC that can only be removed by the NKA, reversal of NCX and other transporters.

Models

To explore the effects of cation retention in thin astrocytic process, a multi-compartmental model was developed consisting of a single synapse surrounded by an astrocytic PsC. Previous imaging studies [37–40] have highlighted the detailed neural/astroglial biological morphology which is comprised of extremely complex geometrical structures. To overcome the computation complexities of modelling the morphology of a synapse, where the influx/efflux of ions is

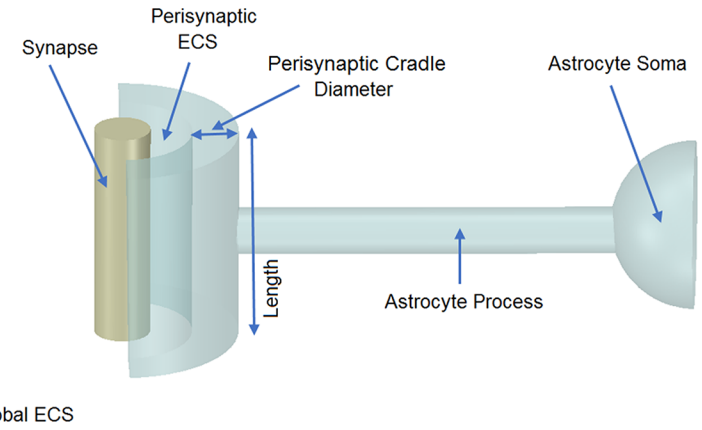

Fig 1. Model morphology. The model consists of a single synapse enwrapped by a single astrocyte. In total there are six compartments, 1) Global Extracellular Space (GECS), 2) Synapse, 3) Perisynaptic Extracellular Space (PsECS), 4) Perisynaptic Cradle, 5) Process, and 6) Astrocyte Soma. Each compartment is modelled as a cylindrical structure except the GECS and soma, which are not given dimensions because ionic concentrations remain constant within these compartments.

https://doi.org/10.1371/journal.pcbi.1006151.g001

3-dimensional, and at the same time capturing the cradle-like structure [38] formed by the PsC around a synapse, we compartmentalise regions of interest using cylindrical arrangements, as shown in Fig 1.

Since the PsC does not completely enwrap the synapse, ions are free to diffuse from the PsECS into the GESC. Note that the ionic concentrations within the astrocyte soma and GECS are held constant but because of electro-diffusion between the GECS and PsECS, the concentration gradient local to the K_{ir} and other channels/pumps will vary. In the absence of data regarding the morphology of the GECS we adopted this approach as we need to have a reference point with fixed baseline ionic concentration levels and resting potential for our model.

Table 1 provides a reference to all morphological values where the diameter of the astrocyte process in this model was 100 nm [41]. From other work [42], both the half cylinder cradle inner diameter and height were assigned the value of 300 nm, the cradle thickness 100 nm and the perisynaptic ESC 30nm. All surface areas and volumes were calculated using these dimensions.

The synapse and PsC contain various ionic channels, exchangers and pumps to provide homeostasis and dynamic exchange of ions between the two cells and extracellular space and are schematically shown in Fig 2 (Note: this diagram does not show the process connection to the astrocyte soma). As we are only considering Na^+ and K^+ dynamics at the PsC our model does not include both the Na-K-Cl cotransporter (NKCC1) and the NCX exchanger; these transporters depend on chloride and calcium respectively, both of which are not investigated in the current model. Furthermore, NKCC1 is not the dominant uptake mechanism for K^+ for ECS K^+ elevation under 10 mM [43].

The complete model contains 7 transport mechanisms which move ions across the membranes. The neuronal model exchanges K^+ and Na^+ with the PsECS via a potassium channel (K_{Neu}) and a sodium potassium pump (NKA_{Neu}), Note: neuronal NKA K^+ binding site is completely saturated, so the only ion that activates neuronal NKA is cytosolic Na^+. The astrocyte exchanges Na^+ and K^+ with the PsECS via a background sodium transport (Na_B), background potassium transport (K_B), potassium inwardly rectifying channel (K_{ir}), sodium-potassium-ATPase (NKA), and a glutamate-sodium-potassium cotransporter (EAAT1/2). I_{KPF} and I_{NaPF} model the current flow of K^+ and Na^+ along the process to the soma. I_{KECSL} models the K^+ current generated by K^+ leaking from the PsECS to the GECS. The mathematical descriptions of these components are now described in detail.

Table 1. Astrocyte morphology.

Parameter	Value	Units	Description	Ref
Lengths:				
d_{IPS}	300×10^{-9}	m	Perisynaptic internal diameter	[42]
d_{EPS}	500×10^{-9}	m	Perisynaptic external diameter	[42]
r_{IPS}	150×10^{-9}	m	Perisynaptic internal radius	[42]
r_{EPS}	250×10^{-9}	m	Perisynaptic external radius	[42]
l_{PS}	300×10^{-9}	m	Perisynaptic length	[42]
d_P	100×10^{-9}	m	Process diameter	[41]
r_P	50×10^{-9}	m	Process radius	[41]
l_P	25×10^{-6}	m	Process length	
d_{Syn}	270×10^{-9}	m	Synapse diameter	
r_{Syn}	135×10^{-9}	m	Synapse radius	
l_{syn}	300×10^{-9}	m	Synapse length	
Areas:				
CSA_{PS}	3.5343×10^{-14}	m^2	Perisynaptic cross sectional area	
SA_{PS}	1.4137×10^{-13}	m^2	Perisynaptic surface area	
CSA_P	7.854×10^{-15}	m^2	Process cross sectional area	
SA_P	7.854×10^{-12}	m^2	Process surface area	
CSA_{Syn}	2.8628×10^{-14}	m^2	Synapse cross sectional area	
SA_{Syn}	1.2723×10^{-13}	m^2	Synapse surface area	
$SA_{PsECS\text{-}GECS}$	1.5715×10^{-14}	m^2	Surface area between PsECS and GECS	
Volumes:				
Vol_{PS}	1.8850×10^{-17}	L	Perisynaptic volume	
Vol_P	1.9635×10^{-16}	L	Process volume	
Vol_{Syn}	8.5883×10^{-16}	L	Synapse volume	
Vol_{PsECS}	2.0145×10^{-18}	L	Perisynaptic ECS volume	

https://doi.org/10.1371/journal.pcbi.1006151.t001

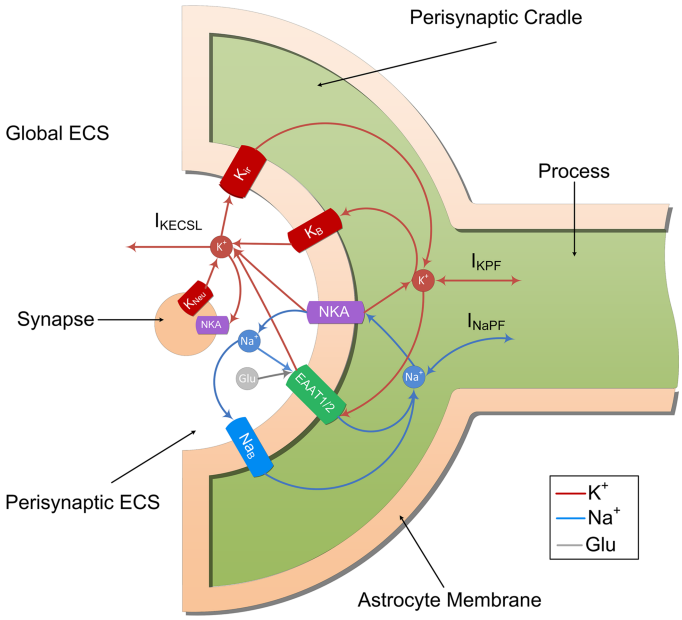

Fig 2. Ion transport machinery of the perisynaptic cradle and synapse.

https://doi.org/10.1371/journal.pcbi.1006151.g002

Astrocyte model

Ion concentrations and membrane voltage. The perisynaptic model comprises five compartments, PsC, perisynaptic extracellular space (PsECS), global extracellular space (GECS), and the astrocyte process and soma. Each of these compartments comprises of three ionic concentrations, K^+, Na^+ and Glu. All channels sensitive to these ions reside on the PsC while the astrocyte process is modelled as a long thin cylindrical channel that restricts the flow of cations within the channel due to ion retention (see later). The kinetic equations for the changes of ionic concentration of each of these ions is given below. Note: z_xFVol_y is used to convert the total ionic current of ion x into a concentration for the volume y, where z_x is the valency of ion x, F is Faradays constant and Vol_y is the volume of compartment y. All initial conditions and parameters for this model are described in Table 2 and Table 3 respectively. The change in PsC K^+ concentration ($[K^+]_{PsC}$) in the PsC is given by:

$$\frac{d[K^+]_{PsC}}{dt} = -\left(\frac{I_{Kir} + I_{KNKA} + I_{KEAAT} + I_{KPF}}{z_K F Vol_{PsC}}\right) \quad (1)$$

where I_{Kir} is the K_{ir} channel current, I_{KNKA} is the K^+ current through the NKA, I_{KEAAT} is the K^+ current created by the glutamate transporter, and I_{KPF} is the K^+ current flowing along the astrocyte process. K^+ changes in the PsECS ($[K^+]_{PsECS}$) is given by:

$$\frac{d[K^+]_{PsECS}}{dt} = -\left(\frac{I_{KECSL} + I_{KNeu} - I_{Km}}{z_K F Vol_{PsECS}}\right) \quad (2)$$

where I_{KECSL} is current due to K^+ leakage from the PsECS to the GECS, I_{KNeu} is the K^+ current from the neurone and I_{Km} is the total K^+ current flowing through the astrocyte membrane. K^+ is held constant in the GECS and astrocyte soma compartments.

Changes in the PsC Na^+ concentration ($[Na^+]_{PsC}$) is given by:

$$\frac{d[Na^+]_{PsC}}{dt} = -\left(\frac{I_{NaB} + I_{NaNKA} + I_{NaEAAT} + I_{NaPF}}{z_{Na} F Vol_{PsC}}\right) \quad (3)$$

where I_{NaB} is a current due to Na^+ influx across the membrane via Na^+ permeable ion channels, this is referred to as background Na^+ channel, I_{NaNKA} is the Na^+ dependent current component of the NKA, I_{NaEAAT} is the Na^+ current component of the glutamate transporter, and I_{NaPF} is the Na^+ current flowing in the astrocyte process. $[Na^+]$ changes in all other compartments are not considered and remain constant.

Changes in the PsECS Glu concentration ($[Glu]_{PsECS}$) is given by:

$$\frac{d[Glu]_{PsECS}}{dt} = -\left(\frac{-I_{GluEAAT}}{z_{Glu} F Vol_{PsECS}}\right) \quad (4)$$

where $I_{GluEAAT}$ is the Glu current component of the glutamate transporter. [Glu] changes in all other compartments are not considered and remain constant. Note: In this work we do not

Table 2. Astrocyte model variables.

Variable	Initial Value	Units	Description	Ref
V_A	-0.09	V	Astrocyte Membrane potential	
$[K^+]_{PsC}$	0.1	M	K^+ concentration in the perisynaptic cradle	[46]
$[Na^+]_{PsC}$	0.015	M	Na^+ concentration in the perisynaptic cradle	[46]
$[K^+]_{PsECS}$	0.003	M	Perisynaptic extracellular K^+ concentration	[46]
$[Glu]_{ECS}$	1×10^{-6}	M	Perisynaptic extracellular Glutamate concentration	[52]

https://doi.org/10.1371/journal.pcbi.1006151.t002

Table 3. Astrocyte model parameters.

Parameter	Value	Units	Description	Ref
V_m	-0.09	V	Astrocyte resting membrane potential	
φ_w	0.267	eV	Well activation energy	[51]
k_B	1.38×10^{-23}	J/K	Boltzmann constant	
R	8.31	J/mol/K	Gas constant	
T	310	K	Temperature	
F	96485	C/mol	Faraday constant	
Q	1.6022×10^{-19}	C	Coulomb	
C_m	0.01	F/m^2	Membrane capacitance	[46]
g_{Kir}	144	S/m^2	K_{ir} channel conductance	[36]
g_K	16.9131	S/m^2	K^+ background transport conductance	
g_{Na}	0.4293	S/m^2	Na^+ background transport conductance	
K_K	0.018	S/m	K^+ Poole-Frenkel channel constant	
K_{Na}	0.018	S/m	Na^+ Poole-Frenkel channel constant	
$PNKA_{max}$	0.1×10^{-5}	mol/m^2	Maximum NKA-ATPase Pump Rate	[46]
K_{Nai}	1.5×10^{-3}	M	Na^+ threshold for NKA-ATPase	
K_{KE}	10×10^{-3}	M	K^+ threshold for NKA-ATPase	
z_K	1		K^+ Valency	
z_{Na}	1		Na^+ Valency	
z_{Glu}	-1		Glu Valency	
$[Glu]_{PsC}$	1.5×10^{-3}	M	Glu concentration in the perisynaptic cradle	[53]
$[H^+]_{PsC}$	60×10^{-9}	M	H^+ Concentration in the perisynaptic cradle	
$[K^+]_{AS}$	0.1	M	K^+ Concentration in the astrocyte soma	
$[Na^+]_{AS}$	0.015	M	Na^+ Concentration in the astrocyte soma	[46]
$[H^+]_{PsECS}$	40×10^{-9}	M	Perisynaptic extracellular H^+ concentration	
$[Na^+]_{PsECS}$	0.145	M	Perisynaptic extracellular Na^+ concentration	[46]
$[K^+]_{GECS}$	0.003	M	Perisynaptic global ECS K^+ concentration	[46]
$[Na^+]_{GECS}$	0.145	M	Perisynaptic global ECS Na^+ concentration	[46]
ε_0	8.85×10^{-12}	F/m	Vacuum permittivity	
ε_r	0.82	F/m	Relative permittivity of brain tissue	[54]
g_{ECS}	3.3	S/m^2	Perisynaptic ECS leak conductance	
α_{EAAT}	0.0032	A/m^2	Glutamate transport fitting parameter	
β_{EAAT}	0.0288	V^{-1}	Glutamate transport fitting parameter	
r_g	5×10^{-7}	M^{-1}	Slope of glutamate uptake	
s_g	9×10^{-6}	M	Threshold for glutamate uptake	

https://doi.org/10.1371/journal.pcbi.1006151.t003

fully model neurone/astrocyte glutamate transport i.e. Glu influx/efflux pathways, therefore, to prevent $[Glu]_{PsECS}$ from draining completely via EAAT1/2 activity which is always active in the inward direction, we simply hold $[Glu]_{PsECS}$ at its initial value when it falls below its initial value.

The membrane voltage of the astrocyte varies according to:

$$C_m \frac{dV_A}{dt} = I_{Km} + I_{Nam} \tag{5}$$

where C_m is the membrane capacitance and I_{Km} and I_{Nam} and is the total current flow across the perisynaptic membrane ion channels and are given by:

$$I_{Km} = I_{KB} + I_{Kir} + I_{KNKA} + I_{KEAAT} \tag{6}$$

$$I_{Nam} = I_{NaB} + I_{NaNKA} + I_{NaEAAT} \tag{7}$$

Inward rectifying potassium channel (Kir). The K_{ir} channel is a voltage dependent ion channel with a high affinity to K^+. The current flow through this channel is given by [36]:

$$I_{KIR} = g_K \sqrt{[K^+]_{PsECS}} (V_A - E_K) SA_{PsC} \tag{8}$$

where g_K is the channel conductance, V_A is the astrocyte membrane voltage, SA_{PsC} is the surface area of the perisynaptic membrane and E_K is the Nernst potential of the channel which is set at 25mV.

Background ion channels (Na_B / K_B). In this model, there are two separate background ion channels for Na^+ and K^+. These channels use the electrochemical gradient between the PsC and ECS resulting in an influx of Na^+ and an efflux of K^+ under normal physiological conditions [21,44]. They were modelled as a simple passive electrochemical gradient dependent channel given by [45]:

$$I_{iB} = g_i (V_A - E_i) SA_{PsC} \tag{9}$$

where i is the ion under consideration, g_i is the channel conductance. Note: the value of g_i is chosen in such a way that at steady state $I_{im} = 0$. V_A is the astrocyte membrane voltage, SA_{PsC} is the surface area of the perisynaptic membrane, and E_i is the channel Nernst potential and is given by:

$$E_i = \frac{RT}{F} \ln\left(\frac{[i^+]_{PsECS}}{[i^+]_{PsC}}\right) \tag{10}$$

Sodium potassium pump (NKA). The NKA exchanges intracellular Na^+ for extracellular K^+ against the gradient of both ions and has a stoichiometry of 3:2. The K^+ current component of the pump is given by [46]:

$$I_{KNKA} = 2\ F\ P_{NKAmax} \frac{[Na^+]_{PsC}^{1.5}}{[Na^+]_{PsC}^{1.5} + K_{Nai}^{1.5}} \frac{[K^+]_{PsECS}}{[K^+]_{PsECS} + K_{KE}} SA_{PsC} \tag{11}$$

and the Na^+ current component of the pump is given by:

$$I_{NaNKA} = -3\ F\ P_{NKAmax} \frac{[Na^+]_{PsC}^{1.5}}{[Na^+]_{PsC}^{1.5} + K_{Nai}^{1.5}} \frac{[K^+]_{PsECS}}{[K^+]_{PsECS} + K_{KE}} SA_{PsC} \tag{12}$$

where P_{NKAmax} is the NKA maximum pump rate, K_{Nai} is the Na^+ threshold of the pump, and K_{KE} is the K^+ threshold of the pump.

Glutamate transporter (EAAT1/2). The EAAT1/2 is responsible for the uptake of extracellular glutamate from the PsECS. Among other ions, it countertransports 1 K^+ and cotransports 3 Na^+ with every glutamate ion [47]. To model this stoichiometry, we adjust the model presented by [48] which describes glutamate uptake by the astrocyte and has a constant transport rate. However, in our model the maximum glutamate transport current (I_{mg}) of the cotransporter is dependent on intra- and extra- cellular levels of K^+, Na^+, H^+, and glutamate.

The K^+ current component of the transporter is given by:

$$I_{KEAAT} = -\frac{I_{mg}}{(1-\exp(r_g s_g - r_g[Glu]_{PsECS}))}\ SA_{PsC} \tag{13}$$

the Glu current component of the transporter is the same magnitude as the K^+ component but in the opposite direction and is given by:

$$I_{GluEAAT} = -I_{KEAAT}\ SA_{PsC} \tag{14}$$

and the Na^+ current component is given by:

$$I_{NaEAAT} = 3\frac{I_{mg}}{(1-\exp(r_g s_g - r_g[Glu]_{PsECS}))}\ SA_{PsC} \tag{15}$$

where I_{mg} is the maximum uptake current of glutamate, r_g is the slope of the glutamate uptake, s_g is the threshold of the glutamate uptake. I_{mg} is given by:

$$I_{mg} = \frac{1}{6}(-\alpha_{EAAT}(\exp(-\beta_{EAAT}(V_A - V_{rev})) - 1)) \tag{16}$$

The constants α_{EAAT} and β_{EAAT} are fitting parameters, V_A is the astrocyte membrane potential and V_{rev} is the EAAT reversal potential, i.e. the driving force.

V_{rev} is dependent on the intra- and extra- cellular concentrations of K^+, Na^+, H^+, and glutamate and is given by:

$$V_{rev} = \frac{RT}{2F}\ln\left(\left(\frac{[Na^+]_{PsECS}}{[Na^+]_{PsC}}\right)^3 \frac{[K^+]_{PsC}}{[K^+]_{PsECS}} \frac{[H^+]_{PsECS}}{[H^+]_{PsC}} \frac{[Glu^+]_{PsECS}}{[Glu^+]_{PsC}}\right) \tag{17}$$

Considering the electrophysiology of the EAAT1/2 reversal potential, we would point out that this potential is defined mainly by glutamate because glutamate rises by 3 orders of magnitude in comparison to Na^+, H^+, K^+ and therefore cannot reverse. Note, as no account is taken of intracellular glutamate, no change in PsC glutamate is calculated and therefore remains constant.

Astrocyte process ionic transport model

Both sides of the bilayer phospholipid membrane surface are negatively charged, however, it has been shown that the distribution of charge is non-uniform at the atomic scale [49]. This non-uniformity gives rise to a potential profile including deep potential wells that can trap ions close to the membrane. Basic quantum mechanics show that regardless of the depth of a well it will have at least one state that can trap the travelling ions. The main effect of the depth of the well is the energy needed for the ion to continue its motion. This means that the ions cannot move easily along the membrane and must "hop" from well to well [49, 50]. Charge hopping transport has been extensively studied in dielectric and semiconductor materials. The present case is particularly complex because of the presence of mobile cations in the cytoplasm, causing the formation of an electrical double layer near the interface between the cytoplasm and the membrane. The negative fixed charge present on the membrane is due to phosphatidylserine (PS) which is composed of phosphatidic acid (PA), with the negatively charged phosphate group attached to the amino acid serine at the hydroxyl end. The associated negative charge will cause cations to move towards the membrane creating a dynamic space charge distribution in the cytoplasm as cations move from one well to an adjacent one; that is, there will be a net movement of cation ions due to the electric field along the length of the process. This

leads to a complex and dynamic 3D potential distribution, which is beyond the scope of this paper. However, in order to investigate the interplay between the retention of cations along the process length and the formations of microdomain at the PsC we draw on a well-established charge hopping model for electrons in dielectrics containing Coulombic trapping centres [51]. In our case, the membrane fixed charge and associated potential wells are deemed analogous to Coulombic trapping centres. The current flow I_{iPF} through the thin process is then represented as:

$$I_{iPF} = K_i \frac{V_A - V_m - V_r}{l} \exp\left[-\frac{Q_i\left(\varphi_{w-}\sqrt{\frac{Q_i(V_A - V_m - V_r)}{l\pi\epsilon}}\right)}{k_B T}\right] CSA_P \quad (18)$$

where K is a constant which represents mobility and concentration of mobile ions, V_m is the resting membrane potential of the astrocyte, φ_w is the well activation energy or potential barrier to ion flow. It has been shown that φ_w lies typically in the range (1–20) × k_BT [51]. and is initially taken as 10 k_BT but the effect of changing φ_w will be considered later; l is the length of the process, Q is the charge on a single ion taken as the charge on an electron, T is the absolute temperature, CSA_P is the cross-sectional area of the process, ϵ is the dynamic permittivity and is given by $\epsilon = \epsilon_0\,\epsilon_r$, where ϵ_0 is the absolute permittivity and ϵ_r is the relative permittivity of the cytoplasm, and k_B is the Boltzmann constant. Note that the potential across the length of the process is assumed linear in this formulation; that is the lateral electric field is constant. The square root term in the argument of the exponential term of Eq 16 represents the field-dependent lowering of the activation energy, φ_w. The 'trapping centres' are assumed to be spaced relatively widely such that their potential distributions do not overlap.

The concentrations of K^+ and Na^+ in the astrocyte soma are held constant but will be continuously changing at the PsC thus establishing a dynamic concentration gradient associated with these cations. Consequently, we formulate a Nernst-like reversal potential for Na^+ and K^+ between the astrocyte soma (AS) and the PsC as:

$$V_r = \frac{RT}{F}\ln\left(\frac{[i]_{AS}}{[i]_{PsC}}\right) \quad (19)$$

where i is the ion under consideration. A schematic of the hopping concept is shown in Fig 3.

Leakage from perisynaptic ECS to global ECS

The diffusion of K^+ between the PsECS and the GECS is modelled as a simple gradient controlled channel and is given by:

$$I_{KECSL} = g_{ECS} E_{ECS} SA_{ECSL} \quad (20)$$

where g_{ECS} is the conductance of the channel, SA_{ECSL} is the surface area between the PsECS and the GECS, and E_{ECS} is the Nernst like potential of the channel given by:

$$E_{ECS} = \frac{RT}{F}\ln\left(\frac{[K^+]_{PsECS}}{[K^+]_{GECS}}\right) \quad (21)$$

Neurone model

The neuronal model utilised in the work consists of the biophysical Hodgkin and Huxley (HH) type model (described in supplementary material S1 Text) [55] with the addition of NKA. All parameter values for the NKA can be found in Table 4.

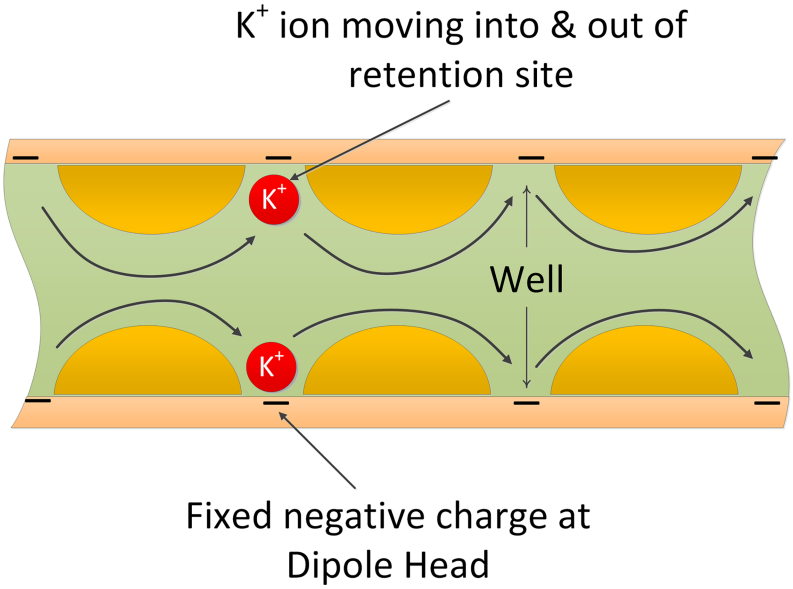

Fig 3. Cross section of a thin process showing charge hopping transport mechanism. The fixed negative charge on the inner membrane surface attracts positively charged cations into wells causing hopping from well to well along the length of the process.

https://doi.org/10.1371/journal.pcbi.1006151.g003

Neurone potassium channel (K_{Neu}). The HH model simulates current flow of K^+ through a voltage gated channel, therefore the current flow of K^+ from the neurone can be modelled as:

$$I_{KNeu} = -\, g_{KNeu} n^4 (V_{Neu} - E_{KNeu}) SA_{Syn} \tag{22}$$

where g_{KNeu} is the maximum K^+ channel conductance, E_{KNeu} is the reversal potential of the potassium channel, V_{Neu} is the membrane voltage of the neurone and SA_{syn} is the surface area of the synapse (neurone parameters described in supplementary material S1 Table).

Neurone sodium potassium pump (NKA_{Neu}). Similar to the astrocytic NKA, the neuronal NKA exchanges intracellular Na^+ for extracellular K^+ against the gradient of both ions and has a stoichiometry of 3:2. The K^+ current component of the pump is given by [46]:

$$I_{KNKANeu} = 2\, F\, P_{NKAmaxNeu} \frac{[Na^+]_{Syn}^{1.5}}{[Na^+]_{Syn}^{1.5} + K_{NaiNeu}^{1.5}} \frac{[K^+]_{PsECS}}{[K^+]_{ECS} + K_{KENeu}} SA_{Syn} \tag{23}$$

where $P_{NKAmaxNeu}$ is the NKA maximum pump rate, K_{NaiNeu} is the Na^+ threshold of the pump, and K_{KENeu} is the K^+ threshold of the pump. Since the neural model does not contain all ion channels necessary for homeostasis, Na^+ changes due to the neuronal NKA pump both inside and outside the synapse are not taken into account. The value of $P_{NKAmaxNeu}$ was chosen in such a way that $I_{KNKANeu} = 0$ at steady state.

Table 4. NKA parameters.

Parameter	Value	Units	Description
$P_{NKAmaxNeu}$	-6.8017×10^{-9}	mol/m^2	Maximum NKA-ATPase Pump Rate
K_{NaiNeu}	1.5×10^{-3}	M	Na^+ threshold for NKA-ATPase
K_{KENeu}	10×10^{-3}	M	K^+ threshold for NKA-ATPase
$[Na^+]_{Syn}$	0.015	M	Na^+ concentration in the synapse

https://doi.org/10.1371/journal.pcbi.1006151.t004

Results

In this section we test the validity of our hypothesis through simulations. The aim is to show that cation retention in thin processes leads to the formation of ionic microdomains at the PsC: Na^+ microdomains were experimentally observed [23] and our hypothesis may very well explain their origin. Specifically, we show that a K^+ microdomain formed at the PsC, provides the driving force for the return of K^+ to the extracellular space for uptake by the neurone, thereby preventing K^+ undershoot. We also show that our model can explain the slow decay of Na^+ at the PsC after a period of glutamate stimulation, which is in strong agreement with experimental observations [23]. Finally, we use our model to predict the dynamic behaviour of ions under more physiological conditions whereby we simulate neuronal co-release of K^+ and glutamate from the presynaptic terminal.

The simulation results presented in this section were obtained using Matlab 2015b 64 bit (Windows version) by Mathworks. The forward Euler method of integration was used for simulation with a fixed time step of $\Delta t = 10\mu s$.

ECS K^+ driven PsC K^+ microdomain formation

To explore how K^+ retention in the astrocyte process gives rise to a K^+ microdomain at the PsC and eliminates K^+ undershoot, several simulations were carried out with the presynaptic neurone stimulated using external currents to produce firing rates of 20Hz, 40Hz, 60Hz and 80Hz. These firing rates are all within physiological frequencies of most cortical pyramidal neurones and fast spiking neurones. The neural stimulus has a duration of ~1 minute where the first 0.1 minute allows the model to reach a steady state condition and the stimulus ceases after 1min. Although this is a long period of time, it allowed an investigation into how extracellular and intracellular ionic concentrations would be affected during a sustained period of neural activity. For each simulation, PsECS [Glu] was held constant at the background level. Fig 4 describes $[K^+]$ and $[Na^+]$ dynamics for each of the 4 different stimuli where it can be seen that neuronal release of K^+ into the PsECS leads to an increase in the astrocyte membrane voltage (V_A in Fig 4A) because of the change in ionic currents through the PsC membrane. It can also be seen that K^+ steadily increases within the PsECS ($[K^+]_{PsECS}$ in Fig 4B) and after a period of ~0.8 minutes it approaches steady state at higher frequencies where the release rate of K^+ by

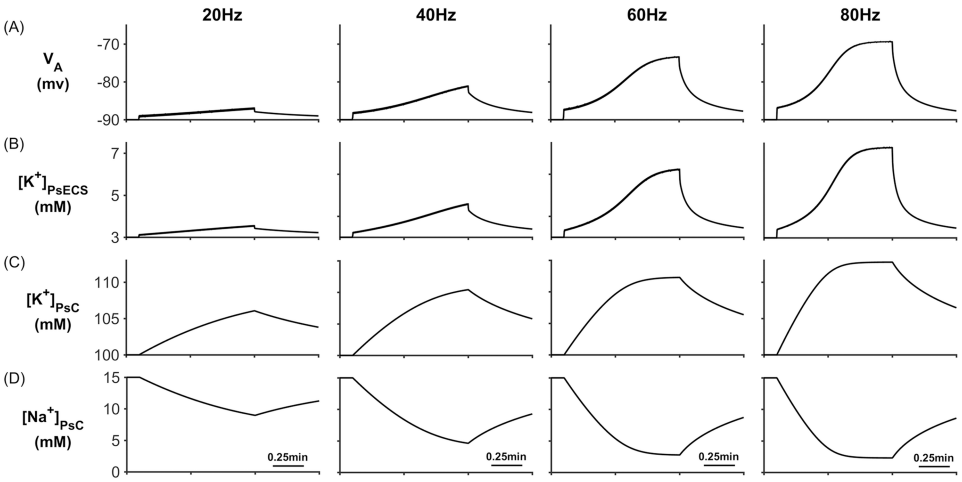

Fig 4. PsC membrane voltages and concentrations against time. (A) Astrocyte membrane voltage (V_A). (B) $[K^+]_{PsECS}$. (C) $[K^+]_{PsC.}$ transient. (D) $[Na^+]_{PsC}$ transient.

https://doi.org/10.1371/journal.pcbi.1006151.g004

the presynaptic neurone equates to the clearance rate by NKA and K_B on both the PsC and the presynaptic terminal, and also K^+ lost into the GECS. It is also worth noting that as the concentration of K^+ increase in the PsC ($[K^+]_{PsC}$ in Fig 4C), the Na^+ concentration with the PsC decrease due to efflux by NKA at the PsC ($[Na^+]_{PsC}$ in Fig 4D). Note: the astrocyte membrane voltage V_A, $[K^+]_{PsECS}$ and $[K^+]_{PsC}$ all increase with the presynaptic neurone firing rate while $[Na^+]_{PsC}$ decreases.

During neural activity, the NKA and K_{ir} channel currents are responsible for K^+ uptake while the background K^+ and KPF currents release K^+ from the PsC. These currents can be seen in Fig 5 where Fig 5B shows that, contrary to the current thinking [56], the NKA is the dominant driving force for K^+ uptake while K_{ir} channel (Fig 5A) is much less so for K^+ clearance: furthermore, clearance by K_{ir} diminishes over time because the changes in the associated reversal potential due to the $[K^+]_{PsC}$ microdomain. Fig 5C shows that I_{KPF} is several orders of magnitude lower than I_{Kir} and therefore this slow leakage of K^+ away from the PsC appears to be a plausible explanation for the emergence of a K^+ microdomain. Note the saturation and subsequent fall off of I_{KB} at higher frequencies is a direct result of the K^+ background reversal potential approaching V_A. This is caused by the rapid build-up of K^+ in the PsECS and cradle. The high frequency oscillatory behaviour which appears as a thickening of Fig 5A–5D is due to the astrocytic response to the pulsed nature of presynaptic neuronal K^+ release. As the potassium in the PsECS fluctuates so does the astrocyte NKA pump and to a lesser extent the astrocyte membrane voltage. These fluctuations in the NKA and membrane voltage are also reflected in Na^+ and K^+ currents. Inserts in Fig 5A–5D, column 1, are used to show detail of astrocyte K^+ current dynamics in response to neurone K^+ release. Note: for clarity only the first column shows this detail as the dynamics for each current is similar for each of the stimulus frequencies.

When the neurone stops releasing K^+ (~ 1min) it quickly flows from the PsECS into the ECS which reduces the K^+ gradient between the PsECS and PsC thereby reducing NKA pump rate, after which a net efflux of K^+ takes place from the stored K^+ in the associated microdomain. This points to a new theory whereby K^+ microdomain formation during neuronal excitation (due to ion retention in the astrocyte process) provides the driver for the return of K^+ to the PsECS, via background K^+ leak and $K_{ir}4.1$ channels, for uptake by the neurone. Fig 6A shows the net transfer of K^+ across the perisynaptic membrane while Fig 6B shows the net

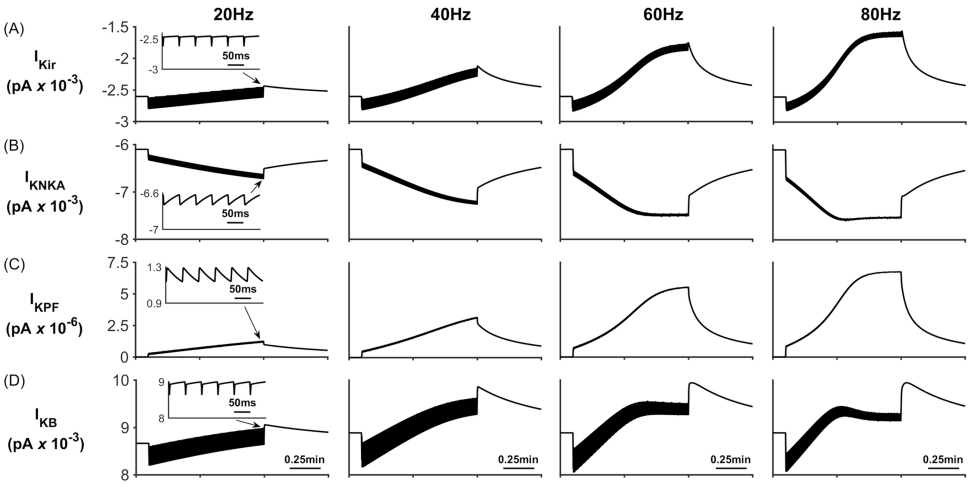

Fig 5. Perisynaptic K^+ currents. (A) K^+ K_{ir} current. (B) K^+ NKA current. (C) K^+ current along the process. (D) Background K^+ current.

https://doi.org/10.1371/journal.pcbi.1006151.g005

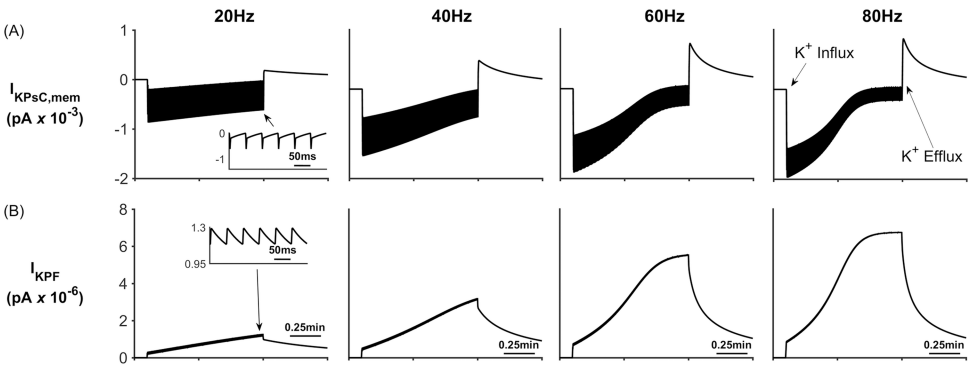

Fig 6. Total perisynaptic membrane K^+ current and K^+ process current. (A) The total K^+ current flowing across the perisynaptic membrane ($I_{KPSC,mem}$). During neural activity (Start = 0.1 min) K^+ in the PsECS is removed by NKA and there is a net influx of K^+. When neural activity stops (1min), K^+ is released back into the PsECS mediated by the background K^+ channel. This influx/efflux can be seen in A column 4. (B) K^+ current flowing along the process (I_{KPF}).

https://doi.org/10.1371/journal.pcbi.1006151.g006

current flow along the process (out of the perisynaptic cradle). During stimulation (0.1 min to 1min) it can be seen that there is a net transfer of K^+ into the perisynaptic cradle across the membrane (Fig 6A). Since the current flowing along the process to the soma (Fig 6B) is 3 orders of magnitude smaller than the currents entering the cradle, there is a net build-up of K^+: essentially a K^+ microdomain forms because of the low conductance pathway from the cradle to the astrocyte soma. Furthermore, this microdomain allows the efflux of K^+ from the PsC into the PsECS after neurone stimulation ceases. This can be seen as a spike like current in Fig 6A after 1min and is more pronounced in the 80Hz simulation.

Fig 7 shows the Na^+ currents for the four different stimulus frequencies. All Na^+ channels, except the NKA (Fig 7B) Na^+ current, result in Na^+ influx to the PsC. When the neurone stops firing there is a net influx of Na^+ into the PsC. The decrease in I_{NaB} (Fig 7A) can be explained as follows: Since I_{NaB} is dependent on the astrocyte membrane potential as well as Na^+ gradient there is a sharp decrease in the current due to the astrocyte membrane potential depolarising.

Glutamate driven PsC Na^+ microdomain formation

As well as K^+ buffering, astrocytes also provide a critical role in glutamate uptake and recycling via the glutamate-glutamine cycle (GGC) [57]. In this simulation, the role of glutamate

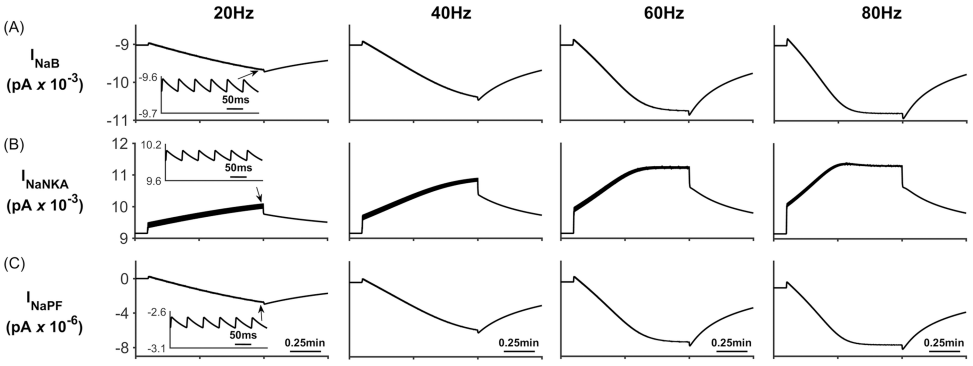

Fig 7. Perisynaptic Na^+ currents. (A) Background Na^+ current. (B) NKA current. (C) Na^+ current along the process. During neural activity, the NKA pumps Na^+ from the cell to allow for K^+ uptake, therefore there is a net decrease in $[Na^+]_{PsC}$. When the neurone stops firing, NKA slows down and there is a net uptake of Na^+ via the remaining channels.

https://doi.org/10.1371/journal.pcbi.1006151.g007

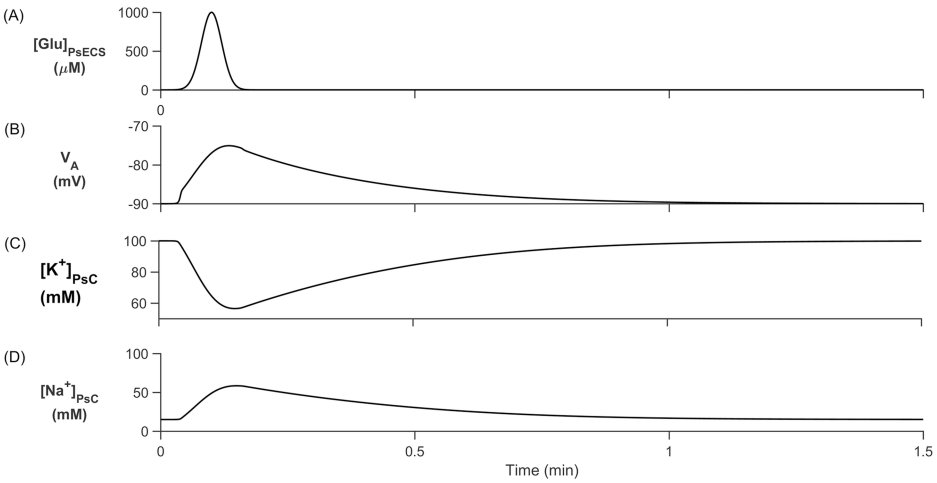

Fig 8. Cell membrane voltage and concentrations. (A) Glutamate is injected into the PsECS with a Gaussian distribution for ~10s with a maximum concentration of 1000μM. (B) PsC membrane voltage depolarises with ionic changes in the PsC. (C) $[Glu]_{PsECS}$ increase causes EAAT1/2 activation and a thereby removing K^+ and (D) the uptake of Na^+.

https://doi.org/10.1371/journal.pcbi.1006151.g008

transport via EAAT1/2 is investigated and results show that the slow leakage of Na^+ ions in the astrocyte process causes Na^+ to increase in the PsC before being returned to the PsECS via the NKA. These results support previously published experimental work [23]: there is no neuronal excitation and therefore the concentration of K^+ in the PsECS is held constant. The concentration of glutamate in the PsECS was modulated using a Gaussian function as shown in Fig 8A. Fig 8B–8D presents the results of the PsC ionic $[K^+]_{PsC}$ and $[Na^+]_{PsC}$ concentrations and membrane voltage, V_A, for this simulation.

From Fig 8C and 8D we clearly see that the $[K^+]_{PsC}$ decreases while $[Na^+]_{PsC}$ increases, this is the opposite dynamics to that observed in Fig 4C and 4D. This is because K^+ in the PsECS is now held constant at 3 mM and therefore all K^+ channels except the NKA and slow leakage through the astrocyte process remove K^+ from the PsC (Fig 9) resulting in a net K^+ efflux. The main driving force behind Na^+ uptake by the PsC is the EAAT1/2 transporter which is also responsible for the removal of glutamate from the PsECS (Fig 10).

During $[Glu]_{PsECS}$ injection, the EAAT1/2 and K_{ir} release K^+ at an accelerated rate. This is opposed by NKA and the transport of K^+ from the astrocyte soma to the PsC. When glutamate falls to baseline levels, the EAAT1/2 and K_{ir} channels quickly revert to their initial rates. NKA and transport of K^+ from the astrocyte soma is then able to establish baseline ionic concentrations at the PsC.

As in the previous simulation, retention of Na^+ ions as they flow within the astrocyte process substantially limits the transport rate of these ions away from the PsC. In this case, Na^+ is restricted and therefore a Na^+ microdomain forms at the PsC. Note: similar to the results presented in [23] there is a long decay (~80s) transient of Na^+ which far outlasts the glutamate signal decrease (Fig 8D) and we propose that this is due to the slow removal of Na^+ by the NKA. These observations could explain previously observed experimental results [23].

ECS K^+ and Glu driven PsC microdomain formation

The previous two simulations have shown that K^+ or Na^+ microdomains form in the PsC when the system is stimulated with PsECS changes in K^+ or Glu respectively. However, while these simulations show that our hypothesis could potentially explain experimental

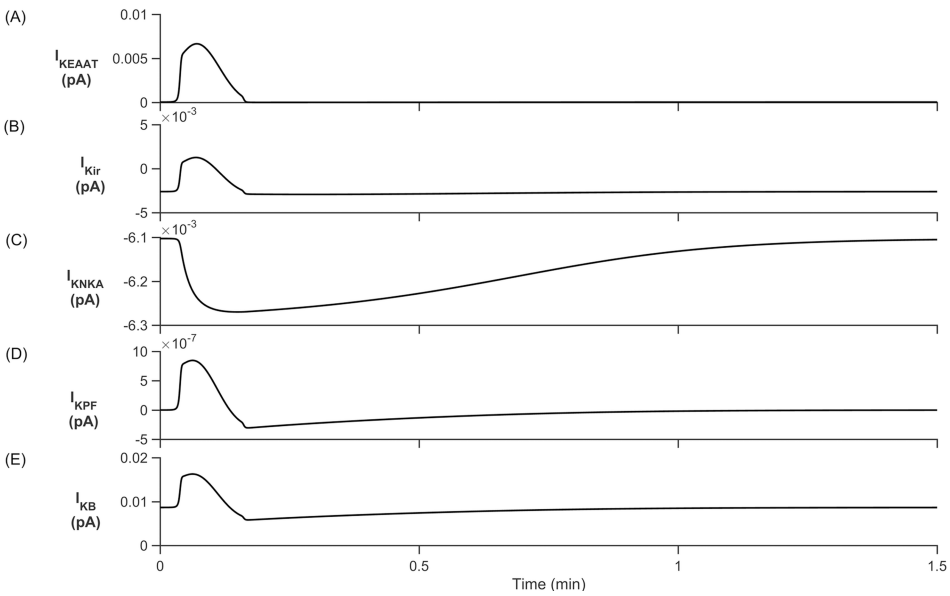

Fig 9. Perisynaptic K^+ currents. (A) K^+ EAAT1/2 current. (B) K^+ K_{ir} current. (C) K^+ NKA current. (D) K^+ current along the process. (E) K^+ background current.

https://doi.org/10.1371/journal.pcbi.1006151.g009

observations, we now wish to use our model to predict ionic dynamics at the PsC under physiological conditions where both K^+ and Glu are released at the presynaptic terminal. In this case K^+ is released by the neurone as before and a 100 μM puff of Glu is released into the PsECS, with each spike event. Presynaptic neurone firing rates are 20Hz, 40Hz, 60Hz and 80Hz, for a period of 0.1min to 1min. The results presented in Fig 11 show that the overall behaviour of the model, i.e. microdomain formation of K^+ in the PsC, occurs. However, the astrocyte membrane voltage V_A oscillates (~7mV amplitude) (Fig 11A) caused by the periodic

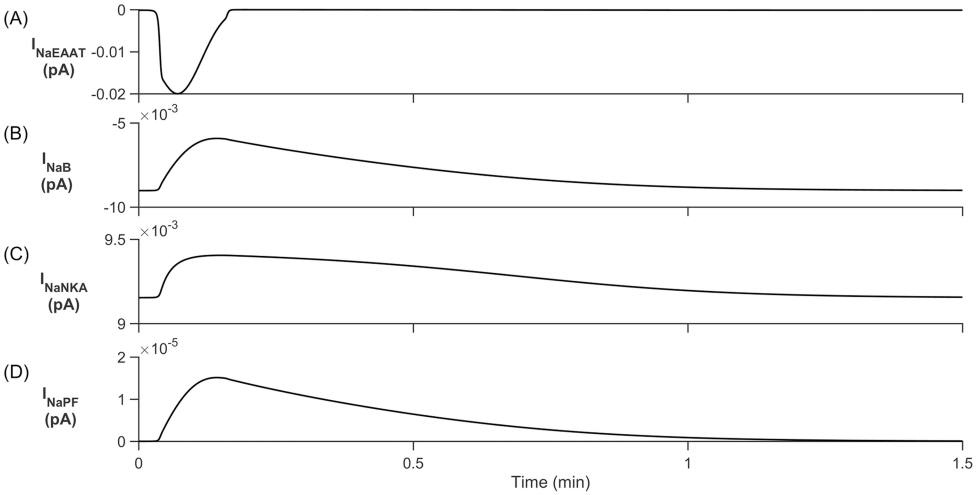

Fig 10. Perisynaptic Na^+ currents. (A) Na^+ EAAT1/2 current. (B) Background Na^+ current. (C) Na^+ NKA current. (D) Na^+ current in the astrocyte process. With the increase of $[Glu]_{PsECS}$, EAAT1/2 transport rate is increased to remove glutamate from the PsECS, in turn Na^+ is taken up. Furthermore, as $[Na^+]_{PsC}$ increases, the rate of Na^+ influx from the background channel decreases. All other channels remove Na^+ until $[Na^+]_{PsECS}$ reaches steady state conditions once again.

https://doi.org/10.1371/journal.pcbi.1006151.g010

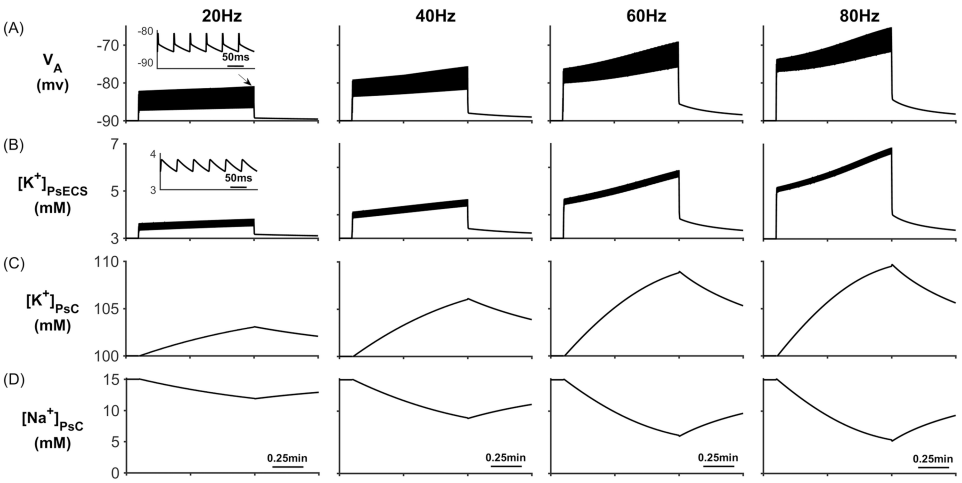

Fig 11. PsC membrane voltages and concentrations against time. (A) Astrocyte membrane voltage (V_A). (B) $[K^+]_{PsECS}$. (C) $[K^+]_{PsC.}$ transient. (D) $[Na^+]_{PsC}$ transient.

https://doi.org/10.1371/journal.pcbi.1006151.g011

reversal of the K_{ir} channel (See Fig 12A). This reversal is caused by the efflux of K^+ via the EAAT1/2 (Fig 12E) channel. Moreover, the dynamic behaviour of the reversal potential of the K_{ir} and V_A continuously cause reversal of the overall polarity (Fig 13), thus causing the K_{ir} channel to periodically reverse direction resulting in an efflux of K^+ into the ECS; this can be seen as oscillations in $[K^+]_{PsECS}$. It can be observed in Fig 11C and 11D that a K^+ microdomain is formed in the PsC and its magnitude increases with frequency while the magnitude of Na^+ reduces. This is due to the behaviour of the K^+ uptake by NKA dominating over the K^+ efflux pathways (See Fig 12).

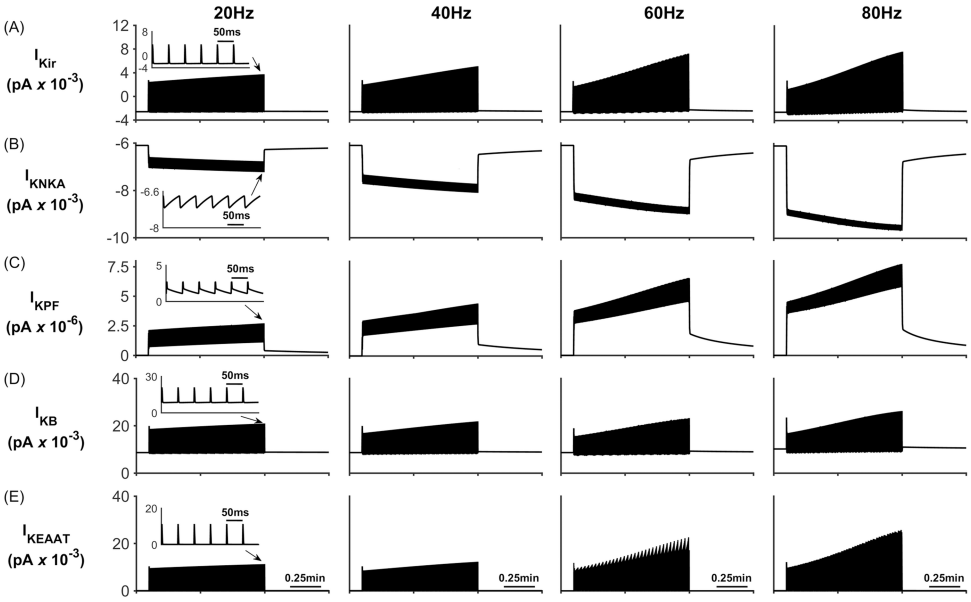

Fig 12. Perisynaptic K^+ currents. (A) K^+ K_{ir} current. (B) K^+ NKA current. (C) K^+ current along the process. (D) Background K^+ current. (E) K^+ EAAT current. Note: similar to the first simulation, as the neurone firing rate increases the magnitude of all currents also increase.

https://doi.org/10.1371/journal.pcbi.1006151.g012

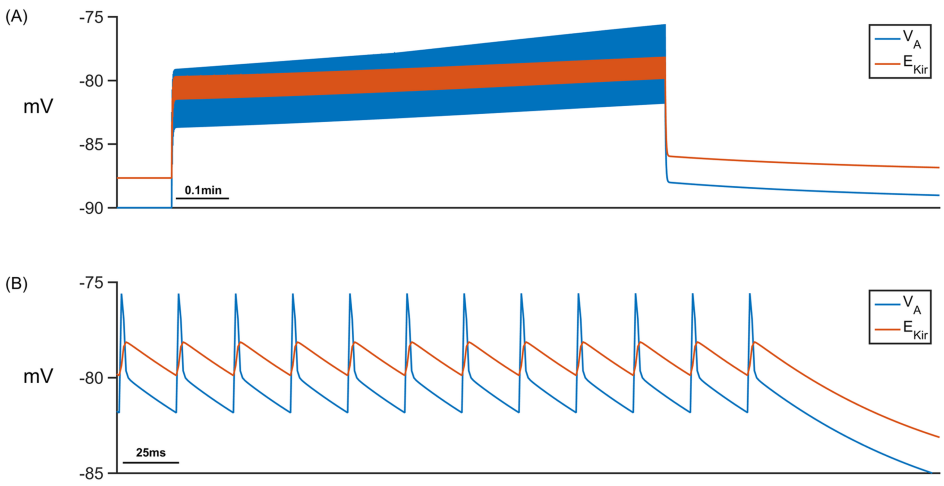

Fig 13. K_{ir} reversal (neurone firing rate: 40Hz). (A) The astrocyte membrane voltage (blue) and the K_{ir} reversal potential continually cross over during neurone stimulation. This results in periodic reversal of the K_{ir} channel. (B) Magnification of A for the last few hundred milliseconds of stimulation.

https://doi.org/10.1371/journal.pcbi.1006151.g013

Fig 14 shows the Na^+ currents for the four different stimulus frequencies. As expected all Na^+ channels on the PsC membrane, except the NKA (Fig 14B) result in Na^+ influx to the PsC. I_{NaEAAT} has a large peak amplitude for a short duration (few milliseconds) due to the EAAT channel slowing down after removal of Glu from PsECS.

Parameter sensitivity

Having analysed the formation of microdomains and model behaviour in the previous three simulations we now explore the sensitivity of the model to model parameters. These parameters are PsC surface area, the maximum NKA pump rate, P_{max}, and the potential barrier to ion flow along the process, φ_w. In these simulations a neuronal firing rate of 40Hz was chosen.

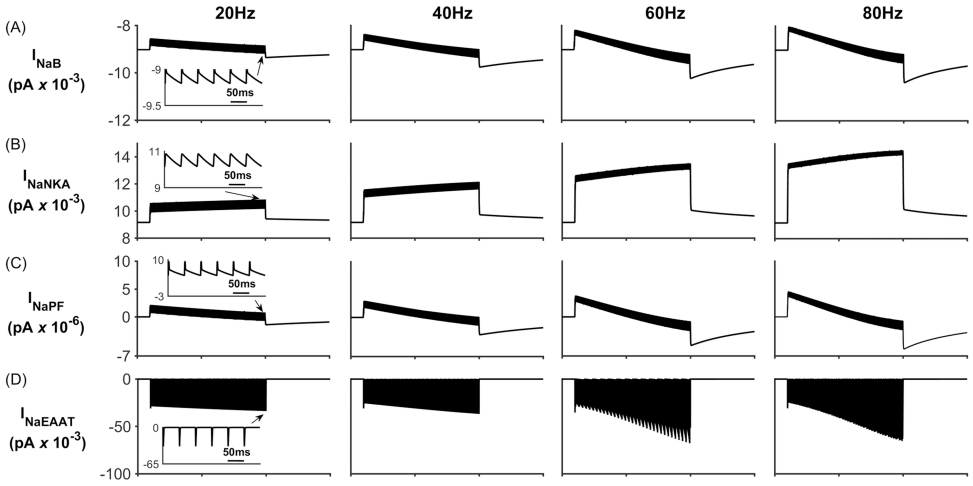

Fig 14. Perisynaptic Na^+ currents. (A) Background Na^+ current. (B) NKA current. (C) Na^+ current along the process. (D) EAAT Na^+ current During neural activity, the NKA pumps Na^+ from the cell to allow for K^+ uptake, therefore there is a net decrease in $[Na^+]_{PsC}$. When the neurone stops firing, NKA slows down and there is a net uptake of Na^+ via the remaining channels.

https://doi.org/10.1371/journal.pcbi.1006151.g014

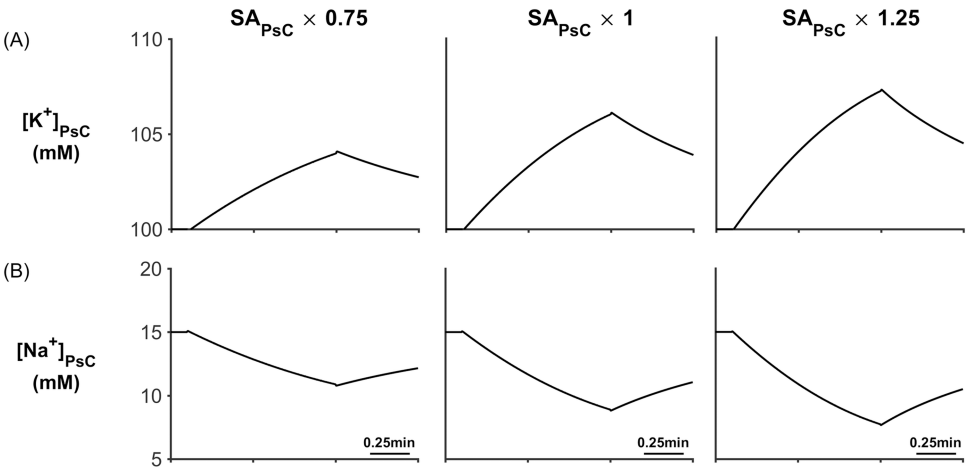

Fig 15. Microdomain formation for different PsC surface areas. (A) PsC K^+ concentration. (B) PsC Na^+ concentration. As the PsC surface area increases so the amplitude of the K^+ microdomain increases and the Na^+ microdomain amplitude decreases.

https://doi.org/10.1371/journal.pcbi.1006151.g015

Microdomain Sensitivity to PsC Surface Area (SA). Three different values of PsC SA were chosen for this simulation; PsC SA × 0.75, PsC SA × 1 and PsC SA × 1.25. The results of these simulations are shown in Fig 15 where it can clearly be seen that the amplitude of the K^+ microdomain increased with PsC SA with a corresponding drop in the concentration of Na^+. Also, the K^+ and Na^+ currents efflux/influx also increased with PsC SA (See Supplementary S1 Fig for the changes in K^+ currents).

Microdomain Sensitivity to $P_{max.}$ Four different values of P_{max} were chosen for this simulation; $P_{max} \times 0.2$, $P_{max} \times 0.5$, $P_{max} \times 1$ and $P_{max} \times 5$. The results of these simulations are shown in Fig 16 where it can clearly be seen that $[K^+]_{PsC}$ and $[Na^+]_{PsC}$ is strongly dependent on P_{max}. Using the P_{max} x 0.2 value causes $[K^+]_{PsC}$ to decrease and $[Na^+]_{PsC}$ to increases and as P_{max} increases, $[K^+]_{PsC}$ begins to form a microdomain with $[Na^+]_{PsC}$ steadily decreasing. From these simulations we can conclude that when the NKA pump rate is low it is no longer the dominant co-transporter and both the EAAT co-transporter and K_{ir} channel dictate $[K^+]_{PsC}$ and $[Na^+]_{PsC}$ dynamics. The opposite is true when the pump rate is large.

Microdomain Sensitivity to $\varphi_{w.}$ In this simulation φ_w was varied from 4 k_BT to 15 k_BT. Fig 17 shows the peak K^+ current along the process for the different values of φ_w. As φ_w is

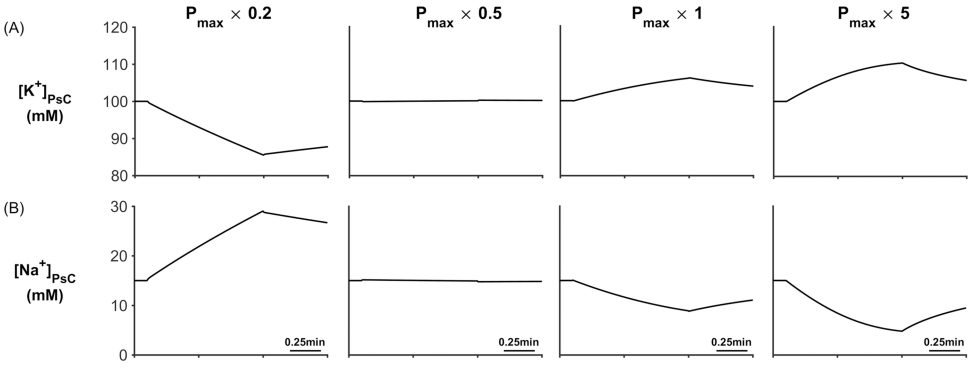

Fig 16. Microdomain formation for different values of NKA maximum pump rate: (A) $[K^+]_{PsC}$ as a function of Pmax and (B) $[Na^+]_{PsC}$ as a function of Pmax.

https://doi.org/10.1371/journal.pcbi.1006151.g016

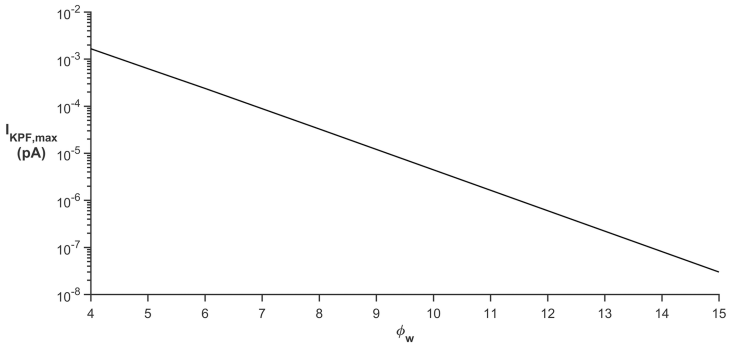

Fig 17. Peak K+ current along the process for different values of φ_w.

https://doi.org/10.1371/journal.pcbi.1006151.g017

decreased, the peak current along the process increases exponentially. Therefore, with decreasing φ_w the formation of a microdomain becomes less likely as $I_{KPF,max}$ is increasing and eventually $I_{KPF,max}$ approaches an electro-diffusion limited model with no likelihood of a microdomain forming at the PsC.

From these simulations it is clear that the mechanism responsible for the formation of microdomains is the well formation along the process which effectively semi-isolate the PsC from the astrocyte soma when φ_w is 10 k_BT or greater. It is also clear that the PsC SA can limit the maximum amplitude of the microdomain concentration. This is due to the increase/decrease of ion channel densities on the membrane of the PsC. Moreover, the NKA maximum pump rate also has an important role in the formation of microdomains whereby if the pump rate is low then K^+ clearance by NKA weakens; effectively these to ion transporters compete to move K^+ and Na^+ ion across the membrane but in opposite directions.

Discussion

Homeostatic control over synaptic cleft, of which K^+ buffering and glutamate uptake is of the most fundamental importance, represent the quintessential function of astroglial cradle formed by the perisynaptic process [7, 8]. Physiological K^+ buffering is essentially K^+ recycling between astroglial and neuronal compartments: NKA-dependent astroglial uptake limits the peak of extracellular K^+ rise, whereas K^+ efflux is imperative for restoration of $[K^+]_i$ in neuronal terminal [3, 10]. Glutamate uptake, as well as glutamate conversion into glutamine and glutamine shuttling to neuronal terminals are regulated by Na^+ concentration in the cytosol of astroglia; astroglial $[Na^+]_i$ in addition controls a multitude of SLC (Solute Carrier) transporters responsible for various homeostatic pathways [20, 21]. Both mechanisms require localisation of ionic signalling within the confines of astroglial synaptic cradle, and indeed local and long-lasting $[Na^+]_i$ transients are routinely recorded from astroglial processes [23, 58]. Molecular machinery responsible for localisation of $[K^+]_i$ and $[Na^+]_i$ increases remains unknown.

Here we table a novel mechanism of localisation of ionic signals in astroglial cells. We propose that ion retention within thin astrocyte processes can give rise to the formation of K^+ and Na^+ microdomains at the PsC. This localisation of astroglial ionic microdomains arises because in thin processes, surface conduction dominates over volume conduction, and because membrane lipids are negatively charged, deep potential wells form near the dipole heads restricting the flow of cations along the process. Therefore, cations must hop from well to well which restricts ion conduction along the membrane. This hopping effectively semi-isolates the PsC from the astrocytic main body allowing the formation of K^+ and Na^+ microdomains at the PsC under different conditions.

We modelled ionic responses of the PsC to the neuronal excitation that results in an increase in K^+ concentration in the synaptic cleft. For the simulation, glutamate in the cleft was held constant at the background level and, during neuronal excitation, K^+ was released into the PsECS leading to a depolarisation in the PsC membrane voltage due to ionic currents flowing through the PsC membrane. The simulations demonstrate that a K^+ microdomain formed at the PsC due to the restricted flow of these ions along the astrocyte process. We further contemplate that the K^+ microdomain provides the driving force for the return of K^+ to the PsECS via background K^+ channels for uptake by the neurone via its NKA. Essentially, K^+ is transiently "stored" at the PsC during neuronal excitation where it decreases the electrochemical gradient of K^+, so reducing inward flow of potassium through K_{ir}; this "stored Potassium" is then available to replenish neuronal K^+ levels when the excitation ceases, thereby preventing K^+ undershoot in the extracellular space. These observations are consistent with in vivo experimental data [59], and partly explain why inward rectifying K^+ channels may play a prominent role for K^+ uptake at large volume glial processes (e.g. terminal endfeet of retinal Muller cells [60] but not at low volume perisynaptic cradles. These results will also necessitate a reappraisal of the mechanisms and role of astrocytes in potassium accumulation during seizure activity [61], especially given the observation that loss of function mutations in the gene encoding $K_{ir}4.1$ are associated with a human epilepsy syndrome [62] and astrocyte $K_{ir}4.1$ expression is decreased in acquired epilepsy models [63]. Moreover, other conditions that have been proposed to be due to abnormalities of potassium homeostasis such as familial hemiplegic migraine are associated with mutations of the gene encoding the alpha2 subunit of NKA, which is predominantly expressed in astrocytes [64].

Our model also shows that the influx of Na^+ ions into the astrocyte process causes a Na^+ microdomain to form at the PsC where the decay rate of Na^+ is governed by the NKA. In this simulation, there is no neuronal excitation and the concentration of glutamate in the cleft was modulated using a Gaussian function and was taken up at the PsC by EAAT1/2. A slow decay of Na^+ was observed after the glutamate uptake ceased which is in strong agreement with experimental observations [21, 23].

In summary, we accept our model for ion retention in thin astrocyte processes requires much more refinement. For example, the main challenge would be to account for the dynamic interaction between the charge present in membrane proteins and the charged ions in the astrocyte medium. Additionally, the dimensions of the astrocyte are such that the membrane proteins are unlikely to be represented by point charges and a more atomistic view of the proteins would need to be found to create a map of the charge distribution at the atomic scale. Also, any simulations would require a large number of atoms to be taken into account to obtain the electrostatic potential profile at the membrane-cytoplasm interface. Once the electrostatic potential in thin process is found and combined with the cation distribution, then the movement of ions can be modelled. Moreover, we have only considered K^+ and Na^+ ions in our model and therefore a more biophysical model would need to consider Ca^{2+} microdomains and Cl^- ion dynamics with the inclusion of the associated membrane transporters such as Sodium/Calcium exchanger and Sodium/Potassium/Chloride cotransporter.

We have assumed throughout the model an infinite GECS but this in reality would not be the case. However more biological data about the shape and size of extracellular spaces and morphology of the perisynaptic cradle would be required before modelling in such a way. Despite this our model does however indicate that the morphological and biophysical properties of the astroglial perisynaptic processes facilitate emergence of Na^+ and K^+ microdomains that are essential for astroglial homeostatic support of synaptic transmission in the central nervous system, and point to new and important implications for potassium homeostasis during pathological activity such as seizures. For example, the long-held view that spatial potassium buffering plays an important role

in seizure activity has been challenged by a number of experimental observations including only a small effect on potassium buffering of knocking out astrocytic gap junction proteins [65], and an antiepileptic effect of gap junction blockers [66]. Indeed, it has been proposed that gap junctions are not necessary for potassium buffering but instead are important for maintaining neuronal metabolism during seizure activity [67]. Our model supports the experimental data and indicates that potassium buffering is a locally restricted phenomenon, and therefore our model challenges the orthodox view of the role of glial spatial potassium buffering during pathological activity. Indeed, our model supports the existence of a mechanism that prevents local potassium depletion during excessive neuronal firing and indicates a novel mechanism by which astrocytes maintain neuronal excitability during pathological activity.

Finally, we would like to point out that ion hopping is a current transport mechanism that involves ions surmounting potential barriers. It is therefore strongly temperature dependent, following Arrhenius behaviour, and has a distinctive temperature and voltage dependence or 'signature' that enables identification against other possible current mechanisms; this may provide a means to test our hypothesis as the kinetics of ionic microdomains formed by Na^+, K^+ or even Cl^- in perisynaptic processes could be quantified in experimental brain slices using respective intracellular probes.

Supporting information

S1 Text. Neurone model. Description of the Hodgkin and Huxley neurone model used in the model simulations.
(DOCX)

S1 Table. Neurone parameters. List of parameter values used by the Neuron Model.
(DOCX)

S1 Fig. Sensitivity to PsC surface area, perisynaptic K^+ currents. (A) K^+ K_{ir} current. (B) K^+ NKA current. (C) K^+ current along the process. (D) Background K^+ current. (E) K^+ EAAT current.
(DOCX)

Author Contributions

Conceptualization: Matthew Walker, Alexei Verkhratsky, Liam McDaid.

Investigation: Kevin Breslin, John Joseph Wade.

Methodology: Kevin Breslin, John Joseph Wade, Bronac Flanagan, Harm Van Zalinge, Steve Hall, Liam McDaid.

Software: Kevin Breslin, John Joseph Wade.

Visualization: John Joseph Wade, Bronac Flanagan.

Writing – original draft: Kevin Breslin, John Joseph Wade, Matthew Walker, Alexei Verkhratsky, Liam McDaid.

Writing – review & editing: Kevin Breslin, John Joseph Wade, KongFatt Wong-Lin, Jim Harkin, Bronac Flanagan, Harm Van Zalinge, Steve Hall, Matthew Walker, Alexei Verkhratsky, Liam McDaid.

References

1. Kettenmann H, Ransom BR editors. Neuroglia. Oxford: Oxford University Press, 2013, p. 864.

2. Verkhratsky A, Butt AM. Glial Physiology and Pathophysiology. Chichester: Wiley-Blackwell, 2013, p. 560.
3. Verkhratsky A, Nedergard M. Physiology of astroglia. Physiol Rev. 2018; 98:239–389.
4. Charvériat M, Naus CC, Leybaert L, Sáez JC, Giaume C. Connexin-Dependent Neuroglial Networking as a New Therapeutic Target. Front Cell Neurosci. 2017; 11: 174. https://doi.org/10.3389/fncel.2017.00174 PMID: 28694772
5. Giaume C, Koulakoff A, Roux L, Holcman D, Rouach N. Astroglial networks: a step further in neuroglial and gliovascular interactions. Nat Rev Neurosci. 2010; 11: 87–99. https://doi.org/10.1038/nrn2757 PMID: 20087359
6. Nedergaard M, Verkhratsky A. Artifact versus reality—how astrocytes contribute to synaptic events. Glia. 2012; 60: 1013–1023. https://doi.org/10.1002/glia.22288 PMID: 22228580
7. Verkhratsky A, Nedergaard M. Astroglial cradle in the life of the synapse. Philos Trans R Soc Lond B Biol Sci. 2014; 369: 20130595, 2014. https://doi.org/10.1098/rstb.2013.0595 PMID: 25225089
8. Verkhratsky A, Nedergaard M. The homeostatic astroglia emerges from evolutionary specialization of neural cells. Philos Trans R Soc Lond B Biol Sci. 2016; 371: 20150428. https://doi.org/10.1098/rstb.2015.0428 PMID: 27377722
9. Kofuji P, Newman EA. Potassium buffering in the central nervous system. Neurosci. 2004; 129(4): 1045–1056.
10. Larsen BR, Assentoft M, Cotrina ML, Hua SZ, Nedergaard M, Kaila K, et al. Contributions of the Na^+/K^+-ATPase, NKCC1, and $K_{ir}4.1$ to hippocampal K^+ clearance and volume responses. Glia 2014; 62: 608–622. https://doi.org/10.1002/glia.22629 PMID: 24482245
11. Larsen BR, MacAulay N. $K_{ir}4.1$-mediated spatial buffering of K^+: experimental challenges in determination of its temporal and quantitative contribution to K^+ clearance in the brain. Channels. 2014; 8(6): 544–550. https://doi.org/10.4161/19336950.2014.970448 PMID: 25483287
12. Boddum K, Jensen TP, Magloire V, Kristiansen U, Rusakov DA, Pavlov I, et al. Astrocytic GABA transporter activity modulates excitatory neurotransmission. Nat Commun. 2016; 7, 13572. https://doi.org/10.1038/ncomms13572 PMID: 27886179
13. Boison D, Chen JF, Fredholm BB. Adenosine signaling and function in glial cells. Cell Death Differ. 2010; 17: 1071–1082. https://doi.org/10.1038/cdd.2009.131 PMID: 19763139
14. Hertz L. The glutamate-glutamine (GABA) cycle: importance of late postnatal development and potential reciprocal interactions between biosynthesis and degradation. Front Endocrinol. 2013; 4: 59.
15. Zhou Y, Danbolt NC. GABA and glutamate transporters in brain. Front Endocrinolo 2013; 4: 165.
16. Hertz L. Possible role of neuroglia: a potassium-mediated neuronal—neuroglial—neuronal impulse transmission system. Nature 1965; 206: 1091–1094. PMID: 5325441
17. Orkand RK, Nicholls JG, Kuffler SW. Effect of nerve impulses on the membrane potential of glial cells in the central nervous system of amphibia. J Neurophysiol. 1966; 29: 788–806. https://doi.org/10.1152/jn.1966.29.4.788 PMID: 5966435
18. Hertz L, Chen Y. Importance of astrocytes for potassium ion (K^+) homeostasis in brain and glial effects of K^+ and its transporters on learning. Neurosci Biobehav Rev. 2016; 71: 484–505. https://doi.org/10.1016/j.neubiorev.2016.09.018 PMID: 27693230
19. Hertz L, Song D, Xu J, Peng L, Gibbs ME. Role of the astrocytic Na^+, K^+-ATPase in K^+ homeostasis in brain: K^+ uptake, signaling pathways and substrate utilization. Neurochem Res. 2015; 40: 2505–2516. https://doi.org/10.1007/s11064-014-1505-x PMID: 25555706
20. Kirischuk S, Parpura V, Verkhratsky A. Sodium dynamics: another key to astroglial excitability? Trends Neurosci. 2012; 35: 497–506. https://doi.org/10.1016/j.tins.2012.04.003 PMID: 22633141
21. Rose CR, Verkhratsky A. Principles of sodium homeostasis and sodium signalling in astroglial. Glia. 2016; 64: 1611–1627. https://doi.org/10.1002/glia.22964 PMID: 26919326
22. Langer J, Stephan J, Theis M, Rose CR. Gap junctions mediate intercellular spread of sodium between hippocampal astrocytes in situ. Glia. 2012; 60: 239–252. https://doi.org/10.1002/glia.21259 PMID: 22025386
23. Kirischuk S, Kettenmann H, Verkhratsky A. Membrane currents and cytoplasmic sodium transients generated by glutamate transport in Bergmann glial cells. Pflug Arch Eur J Phy. 2007; 454: 245–252.
24. Vandenberg RJ, Ryan RM. Mechanisms of glutamate transport. Physiol Rev. 2013; 93: 1621–1657. https://doi.org/10.1152/physrev.00007.2013 PMID: 24137018
25. Palygin O, Lalo U, Verkhratsky A, Pankratov Y. Ionotropic NMDA and $P2X_{1/5}$ receptors mediate synaptically induced Ca^{2+} signalling in cortical astrocytes. Cell Calcium. 2010; 48: 225–231. https://doi.org/10.1016/j.ceca.2010.09.004 PMID: 20926134

26. Reyes RC, Verkhratsky A, and Parpura V. TRPC1-mediated Ca^{2+} and Na^{+} signalling in astroglia: Differential filtering of extracellular cations. Cell Calcium. 2013; 54(2): 120–125. https://doi.org/10.1016/j.ceca.2013.05.005 PMID: 23764169

27. Verkhratsky A, Kirchhoff F. NMDA receptors in glia. Neuroscientist 2007; 13: 28–37. https://doi.org/10.1177/1073858406294270 PMID: 17229973

28. Verkhratsky A, Reyes RC, Parpura V. TRP channels coordinate ion signalling in astroglia. Rev Physiol Biochem Pharmacol. 2014; 166: 1–22. https://doi.org/10.1007/112_2013_15 PMID: 23784619

29. Minelli A, Castaldo P, Gobbi P, Salucci S, Magi S, Amoroso S. Cellular and subcellular localization of Na^{+}–$Ca2^{+}$ exchanger protein isoforms, NCX1, NCX2, and NCX3 in cerebral cortex and hippocampus of adult rat. Cell Calcium. 2007; 41(3): 221–234. https://doi.org/10.1016/j.ceca.2006.06.004 PMID: 16914199

30. Parpura V. Verkhratsky A. Homeostatic function of astrocytes: Ca(2+) and Na(+) signalling. Translational neuroscience. 2012; 3: 334–344. https://doi.org/10.2478/s13380-012-0040-y PMID: 23243501

31. Grosche J, Matyash V, Möller T, Verkhratsky A, Reichenbach A, Kettenmann H. Microdomains for neuron–glia interaction: parallel fiber signaling to Bergmann glial cells. Nat Neurosci. 1999; 2: 139–143. https://doi.org/10.1038/5692 PMID: 10195197

32. Langer J, Gerkau NJ, Derouiche A, Kleinhans C, Moshrefi-Ravasdjani B, Fredrich M, et al. Rapid sodium signaling couples glutamate uptake to breakdown of ATP in perivascular astrocyte endfeet. Glia 2017; 65: 293–308. https://doi.org/10.1002/glia.23092 PMID: 27785828

33. Elul R. Fixed charge in the cell membrane. J Physiol. 1967; 189(3): 351–365. PMID: 6040152

34. Alberts B, Johnson A, Lewis J, Raff M, Roberts K, Walter P. The lipid bilayer. In molecular biology of the cell. 4th edition. New York: Garland Science; 2002.

35. Fadeel B, Xue D. The ins and outs of phospholipid asymmetry in the plasma membrane: roles in health and disease. Crit Rev Biochem Mol Biol. 2009; 44(5): 264–277. https://doi.org/10.1080/10409230903193307 PMID: 19780638

36. Witthoft A, Filosa JA, Karniadakis GE. Potassium buffering in the neurovascular Unit: Models and sensitivity. Biophys J. 2013; 105: 2046–2054. https://doi.org/10.1016/j.bpj.2013.09.012 PMID: 24209849

37. Patrushev I, Nikolay Gavrilov N, Turlapov V, Semyanov A. Subcellular location of astrocytic calcium stores favors extrasynaptic neuron–astrocyte communication. Cell Calcium. 2013; 54: 343–349. https://doi.org/10.1016/j.ceca.2013.08.003 PMID: 24035346

38. Lushnikova I, Skibo G, Muller D, Nikonenko I. Synaptic potentiation induces increased glial coverage of excitatory synapses in CA1 hippocampus. Hippocampus. 2009; 19: 753–762. https://doi.org/10.1002/hipo.20551 PMID: 19156853

39. Witcher MR., Kirov SA, Harris KM. Plasticity of perisynaptic astroglia during synaptogenesis in the mature rat hippocampus. Glia. 2007; 55: 13–23. https://doi.org/10.1002/glia.20415 PMID: 17001633

40. Xu-Friedman MA, Harris KM, Regehr WG. Three-dimensional comparison of ultrastructural characteristics at depressing and facilitating synapses onto cerebellar Purkinje cells. J Neurosci. 2001; 21(17): 6666–6672. PMID: 11517256

41. Derouiche A, Frotscher M. Peripheral astrocyte processes: monitoring by selective immunostaining for the actin-binding ERM proteins. Glia. 2001; 36: 330–341. PMID: 11746770

42. Ribrault C, Sekimoto K, Triller A. From the stochasticity of molecular processes to the variability of synaptic transmission. Nat Rev. 2011; 12: 375–387.

43. Walz W, Hertz L. Intense furosemide-sensitive potassium accumulation in astrocytes in the presence of pathologically high extracellular potassium levels. J Cereb Blood Flow Metab. 1984; 4: 301–304, https://doi.org/10.1038/jcbfm.1984.42 PMID: 6725441

44. Ryoo K, Park JY. Two-pore domain potassium channels in astrocytes. Exp Neurobiol. 2016; 35(5): 222–232.

45. Sterratt D, Graham B, Gillies A, Willshaw D. Principles of computational modelling in neuroscience. 1st ed. United Kingdom: Cambridge University Press; 2011.

46. Halnes G, Østby I, Pettersen KH, Omholt SW, Einevoll E. Electrodiffusive model for astrocytic and neuronal ion concentration dynamics. PLoS Comp Biol. 2013; 9(12): e1003386.

47. Grewer C, Gameiro A, Rauen T. SLC1 glutamate transporters. Pflug Arch Eur J Phy. 2014; 466(1): 3–24.

48. Blanchard S, Saillet S, Ivanov A, Benquet P. Bénar C-G, Pélégrini-Issac M. et al. A New computational model for neuro-glio-vascular coupling: astrocyte activation can explain cerebral blood flow nonlinear response to interictal events. Plos One. 2016; 11(2): e0147292 https://doi.org/10.1371/journal.pone.0147292 PMID: 26849643

49. Klausen LH, Fuhs T, Dong M. Mapping surface charge density of lipid bilayers by quantitative surface conductivity microscopy. Nat Commun. 2016; 7: 12447. https://doi.org/10.1038/ncomms12447 PMID: 27561322

50. Pekker M, Shneider MN. Interaction between electrolyte ions and the surface of a cell lipid membrane. J Phys Chem Biophys. 2015; 5(2): https://doi.org/10.4172/2161-0398.1000177

51. Frenkel J. On pre-breakdown phenomena in insulators and electronic semi-conductors. Phys Rev. 1938; 54: 647–648.

52. Anderson CM, Swanson RA. Astrocyte glutamate transport: Review of properties, regulation, and functions. Glia. 2000; 32: 1–14. https://doi.org/10.1002/1098-1136(200010)32:1<1::AID-GLIA10>3.0.CO;2-W PMID: 10975906

53. Attwell D, Barbour B, Szatkowski M. Nonvesicular release of neurotransmitter. Neuron 1993; 11 (3):401–407. PMID: 8104430

54. Foster KR, Schepps JL, Stoy RD, Schwan HP. Dielectric properties of brain tissue between 0.01 and 10 GHz. Phys Med Biol. 1979; 24(6): 1177–1187. PMID: 531093

55. Hodgkin AL, Huxley AF. A quantitative description of membrane current and its application to conduction and excitation in nerve. J Physiol. 1952; 117(4): 500–544. PMID: 12991237

56. Butt M, Kalsi A. Inwardly rectifying potassium channels (Kir) in central nervous system glia: a special role for Kir4.1 in glia functions. J Cell Mol Med. 2006; 10(1): 33–44. https://doi.org/10.1111/j.1582-4934.2006.tb00289.x PMID: 16563220

57. Schousboe A, Scafidi S, Bak LK, Waagepetersen HS, McKenna MC. Glutamate metabolisim in the brain focusing on astrocytes Adv Neurobiol. 2014; 11: 13–30. https://doi.org/10.1007/978-3-319-08894-5_2 PMID: 25236722

58. Langer J, Rose CR. Synaptically induced sodium signals in hippocampal astrocytes in situ. J Physiol. 2009; 587: 5859–5877. https://doi.org/10.1113/jphysiol.2009.182279 PMID: 19858225

59. D'Ambosio R, Gordon DS, Winn HR. Differential role of KIR channel and Na^+/K^+-pump in the regulation of extracellular K^+ in rat hippocampus. J Neurophysiol. 2001; 87: 87–102.

60. Brew H, Gray PTA, Mobbs P, Attwell D. Endfeet of retinal glial cells have higher desities of ion channels that mediate K+ buffereing. Nature. 1986; 324: 466–468. https://doi.org/10.1038/324466a0 PMID: 2431322

61. Grigorovsky V, Bardakjian BL. Effects of astrocytic mechanisms on neuronal hyperexcitability. Conf Proc IEEE Eng Med Biol Soc. 2014; 4880–4883. https://doi.org/10.1109/EMBC.2014.6944717 PMID: 25571085

62. Reichold M, Zdebik AA, Lieberer E, Rapedius M, Schmidt K, Bandulik S, et al. KCNJ10 gene mutations causing EAST syndrome (epilepsy, ataxia, sensorineural deafness, and tubulopathy) disrupt channel function. Proc Natl Acad Sci U S A. 2010; 107(32): 14490–14495. https://doi.org/10.1073/pnas.1003072107 PMID: 20651251

63. Ivens S, Kaufer D, Flores LP, Bechmann I, Zumsteg D, Tomkins O, et al. TGF-beta receptor-mediated albumin uptake into astrocytes is involved in neocortical epileptogenesis. Brain. 2017; 130(pt2): 535–547.

64. De Fusco M, Marconi R, Silvestri L, Atorino L, Rampoldi L, Morgante L, et al. Haploinsufficiency of ATP1A2 encoding the Na^+/K^+ pump alpha2 subunit associated with familial hemiplegic migraine type 2. Nat Genet. 2003; 33(2): 192–196. https://doi.org/10.1038/ng1081 PMID: 12539047

65. Wallraff A, Köhling R, Heinemann U, Theis M, Willecke K, Steinhäuser C. The impact of astrocytic gap junctional coupling on potassium buffering in the hippocampus. J Neurosci. 2006 26: 5438–5447. https://doi.org/10.1523/JNEUROSCI.0037-06.2006 PMID: 16707796

66. Samoilova M, Wentlandt K, Adamchik Y, Velumian AA, Carlen PL. Connexin 43 mimetic peptides inhibit spontaneous epileptiform activity in organotypic hippocampal slice cultures. Exp Neurol. 2008; 210(2): 762–775. https://doi.org/10.1016/j.expneurol.2008.01.005 PMID: 18284929

67. Rouach N, Koulakoff A, Abudara V, Willecke K, Giaume C. Astroglial metabolic networks sustain hippocampal synaptic transmission. Science. 2008; 322(5907): 1551–1555). https://doi.org/10.1126/science.1164022 PMID: 19056987